Electrochemistry

The Electrochemical Society of Japan

Received: September 20, 2013
Accepted: October 25, 2013
Published: December 27, 2013

http://dx.doi.org/10.5796/electrochemistry.82.25
JOI:DN/JST.JSTAGE/electrochemistry/82.25

Article *Electrochemistry*, **82(1)**, 25–30 (2014)

SnSe Thin Film Electrodes Prepared by Vacuum Evaporation: Enhancement of Photoelectrochemical Efficiency by Argon Gas Condensation Method

Nordin SABLI,[a] Zainal Abidin TALIB,[a,*] Wan Mahmood Mat YUNUS,[a] Zulkarnain ZAINAL,[b] Hikmat S. HILAL,[c] and Masatoshi FUJII[d]

[a] *Department of Physics, Faculty of Science, Universiti Putra Malaysia, 43400 UPM Serdang, Selangor, Malaysia*
[b] *Department of Chemistry, Faculty of Science, Universiti Putra Malaysia, 43400 UPM Serdang, Selangor, Malaysia*
[c] *Department of Chemistry An-Najah National University, PO Box 7, Nablus, West Bank, Palestine*
[d] *Department of Molecular Science, School of Medicine, Shimane University, Izumo, Shimane, 693-8501, Japan*

* *Corresponding author: zainalat@upm.edu.my*

ABSTRACT

The effect of argon gas condensation (AGC) on crystallinity, surface morphology and photoelectrochemical (PEC) characteristics of SnSe thin films, prepared by thermal vacuum deposition onto ITO/glass substrates, has been investigated. The focal theme was to improve growth process of SnSe thin films and consequently enhance their PEC characteristics, by including argon gas during film manufacturing. For comparison purposes, the films grown With- and Without-AGC were characterized using various techniques such as X-ray diffractometry, UV-VIS spectroscopy, and SEM. The results indicate enhancement in film crystallinity and surface morphology by inclusion of argon gas. Such enhancement has been attributed to slower deposition rate due to argon gas presence. Photoelectrochemical property of SnSe thin film electrodes was studied using linear sweep voltammetry in dark and under illumination. The With-AGC electrodes showed higher photoactivity than the Without-AGC counterparts. Enhancement of PEC characteristics of SnSe With-AGC thin film electrodes is consistent with their crystallinity and surface uniformity. Inclusion of AGC in thermal vacuum deposition processes is potentially valuable to prepare enhanced SnSe thin film electrodes even without the need for further treatment such as etching or annealing.

Keywords : Argon Gas Condensation, Photoelectrochemical, Photoactivity, Tin Selenide

1. Introduction

Fossil fuels are being considered as a real threat to human being, due to their hazardous outcomes and to their non-renewable nature. Renewable energy, which is based on solar energy, is a novel alternative, and seems to be a promising candidate to solve future energy problems. Photovoltaic (PV) systems were investigated and are currently being used at commercial scale, but they are costly and demand special conditions to prepare. As an alternative, however, PEC cells are simple to construct, economic in materials consumption and can be used for both solar-to-electrical energy and solar-to-chemical energy conversion processes. Intensive research is globally underway to use such conversion systems for energy production. However, PEC energy conversion systems still have limitations to overcome including electrode low efficiency and stability. The PEC efficiency critically depends on the quality of semiconductor (SC) surface at the solid/redox couple interface.[1,2] Hence, from material science point of view, controlling the microstructure of semiconductor surface is of main importance to produce high performance PEC systems with high conversion efficiency and high stability.[3] Thus, grain size distribution, grain shape, elemental composition, internal structure and surface chemical condition are important features for the SC thin film electrode. Different techniques have been investigated to control such features,[4–12] one of which is the film preparation method. The AGC thermal evaporation of a material has many advantages over other processing methods, including (i) potential deposition of many alloys with grain sizes less than 100 nm, (ii) shape similarity and narrow size distribution of particles, and (iii) easy control of film characteristics. AGC has been successfully utilized in metal and nano-cluster depositions.[13] The technique has also been effectively used to enhance metal chalcogenide thin film electrodes in PEC systems, such as CuZnSnSe electrodes.[14] Selection of the proper semiconductor for a given PEC system is also a critical issue. Since SnSe is chemically stable in acid or alkaline media, with a band gap value 1.21 eV,[15–18] it is worth to use it in PEC systems. Thus, SnSe thin films can be potential candidates for PEC solar cells, should their characteristics be well controlled. Due to the toxic nature of Se compounds, stabilizing SnSe film electrodes is a necessary task to achieve.

Different methods to prepare SnSe nano-films have been described.[7] The focal theme of this work is to improve the growth processes of SnSe thin films by including AGC. This report is the first to describe preparing SnSe film electrodes by AGC and studying the consequences on their characteristics. Effects of using AGC on structural, morphological, optical properties and photoactivity of the films have been investigated.

2. Experimental

2.1 Chemicals

$K_3Fe(CN)_6$ and $K_4Fe(CN)_6{\cdot}H_2O$ were purchased from Sigma Aldrich. HCl was purchased from Friendmann Schmidt Chemical. Organic solvents, methanol and 2-propanol, were purchased from Merck KGaA and HmbG Chemicals respectively. Starting materials tin and selenium were purchased from Alfa Aesar with nominal purity 99.8% and 99.5% respectively.

2.2 Equipment

XRD patterns of prepared starting powders and thin films were measured on an XPERT-PRO X-Ray diffractometer using Cu Kα ray ($\lambda = 1.54056$ Å). Surface morphology was studied by recording

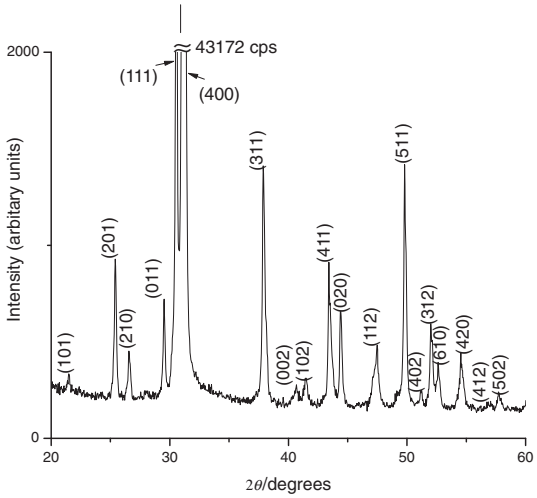

Figure 1. XRD pattern of synthesized SnSe powder.

images on an FESEM on Nova Nano SEM 230 equipment. Optical properties were recorded using a UV-VIS-NIR spectrometer for absorption and reflectance spectra in the range 400–800 nm.

2.3 Synthesis of SnSe compound

The evaporation source of SnSe compound was prepared using the melt-quenching method, as follows: the elements Sn and Se were weighed with a stoichiometric 1:1 nominal molar ratio, mixed and placed inside a sealed vacuum quartz ampoule. The ampoule was heated to 1000°C, which is higher than the SnSe melting point (880°C) according to Tin-Selenium phase diagram.[19] The furnace temperature was gradually increased from room temperature at a ramp rate of 5°C/min. After reaching the 1000°C temperature, the furnace was rocked for 48 hours to ensure complete mixing and sample homogeneity. Rocking frequency was set at 20 second/cycle with 45° angles. The heated ampoule was then quenched in liquid nitrogen to obtain the desired stoichiometry.

The prepared sample blocks were taken and ground to powder using a mortar and a pestle. Figure 1 shows the XRD pattern of the synthesized powder. Since the peaks well matched with JCPDS Card number 98-009-1204, the synthesized powder was identified as polycrystalline SnSe. The peak intensity of (400) plane shows much stronger than that of the reference, due to enhanced crystallinity. The XRD pattern is consistent with earlier reports.[7] The prepared SnSe powder was used as a source material for the thin film electrodes by vacuum thermal evaporation With- and Without-AGC, as described below.

2.4 Preparation of SnSe thin film photo-electrode

The prepared SnSe powder (0.10 g) was placed in a molybdenum evaporation boat. In order to obtain strong adherence and film uniformity, substrates of highly conductive ITO/glass slides, were pre-cleaned prior to deposition. The multi-step cleaning process involved the following (i) washing with soap, (ii) rinsing with distilled water, (iii) washing with methanol, (iv) rinsing again with distilled water, (v) soaking in dilute HCl 10% (v/v) for 10 s, (vi) rinsing with distilled water, (vii) washing with methanol, (viii) rinsing again with distilled water, and (ix) rinsing with boiling isopropyl alcohol before drying.

Two types of deposition experiments were performed; one using AGC and the other without ACG. Other parameters (preparation procedure of substrate, base pressure, pre-heat temperature and time, and deposition time) were kept the same. The substrates were mounted on a mask that was placed 14 cm above the boat. The set was then covered with a bell jar and evacuated to a vacuum of 5×10^{-4} Pa. In the absence of AGC, the vacuum chamber pressure was kept at 5×10^{-4} Pa, whereas in presence of the AGC, the pressure was kept at 7.5×10^{-2} Pa with an argon flow rate 5.0 cm^3/min. The argon gas was introduced into the chamber via an inlet tube having a nozzle 0.5 mm in diameter. The nozzle was mounted near the evaporation boat, and its outlet direction was pointed towards the substrate. Prior to deposition, the boat containing SnSe powder was pre-heated for 1 hour at a temperature lower than the melting point (<880°C). By gradually increasing the applied current, the SnSe powder melted, evaporated from the boat and deposited on the substrate, which was kept unheated during the evaporation process. Deposition time needed to completely melt the 0.1 g SnSe powder was 5 s for both With-AGC and Without-AGC.

2.5 PEC experiment

PEC experiments were performed using $[Fe(CN)_6]^{3-}$/$[Fe(CN)_6]^{4-}$ redox system, by running linear sweep voltammetry between +1.0 V and −0.4 V with a scan speed of 20 mV/s using a PGSTAT 101 Potentiostat. 0.05 M of $K_3Fe(CN)_6$ and 0.05 M of $K_4Fe(CN)_6{\cdot}H_2O$ in distilled water were used as electrolyte solution. A conventional three-electrode cell, equipped with a platinum counter electrode and an Ag/AgCl reference electrode, was used. To remove oxygen from the electrolyte, N_2 gas was bubbled through the solution for more than 15 min before measurement. An Osram halogen lamp was used as a light source. The light intensity at the working electrode was measured to be 0.1 W/cm^2 by a pyranometer (LI-200; Li-Cor, USA). In-dark experiments were performed by switching off the light source and covering the system with a black thick cardboard. Electrode photoactivity was assessed by measuring the photo current density vs. potential (J-V) plots. PEC electrode stability testing was performed by monitoring the photocurrent for 7 hours at an applied potential 0.0 V (vs. Ag/AgCl reference electrode) under illumination intensity 0.1 W/cm^2.

3. Results and Discussion

3.1 XRD analysis for thin film

The XRD patterns recorded for the as-deposited SnSe thin films using both methods are presented in Fig. 2. The XRD patterns indicate the formation of poly-crystals with orthorhombic structure. The peak patterns are well matched with JCPDS Card number 98-009-1204. The prominent Bragg reflection occurred at $2\theta = \sim 30°$ corresponding to (111) diffraction. A similar preferred orientation along the (111) plane in SnSe film was reported by Kumar et al.[20] and by Zulkarnain et al.[21]

The XRD results are summarized in Table 1. The (111) inter-planar distance (d) values for With- and Without-AGC films are compared with the standard data (JCPDS Card number 98-009-1204). The crystallite size values, Table 1, were calculated from the FWHM values of the highest intensity peak (111) using the Scherrer's equation. Values of full width at half maximum (FWHM) for all peaks for the With-AGC film are narrower than those for Without-ACG film, which means that the former film is more crystalline than the latter. This is presumably due to the lower deposition rate in case of the AGC system. Higher crystallinity is expected as crystal components have more time to deposit into more uniform clusters. Inert gas slows down the precipitation process, as the gaseous species collide with argon atoms and lose their kinetic energy, as reported earlier for other systems.[22] The crystallinity improvement associated with the With-AGC method here resembles the annealing effect on film characteristics reported earlier.[23,24] Table 1 shows that the With-AGC film involved larger crystallites (12.5 nm) than those in the Without-AGC film (10.8 nm). This is understandable, as larger crystallites are expected from by lower deposition rate in case of the With-AGC films.

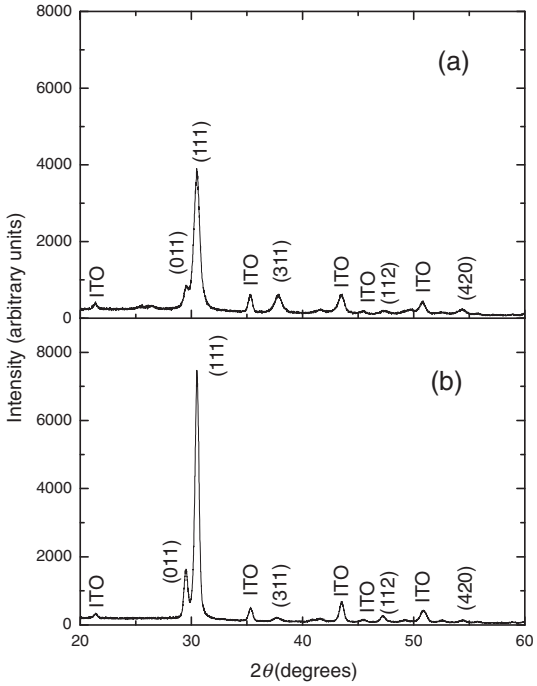

Figure 2. XRD patterns of SnSe thin films (a) Without-AGC method and (b) With-AGC method.

Table 1. Comparison of various structural parameters for With-AGC and Without-AGC SnSe films with the standard data base.

Item	Angle (2θ)	Plane (*hkl*)	d (Å)	FWHM (°)	Crystallite size (nm)
Without AGC	30.5	111	2.929	0.8089	10.8
With AGC	30.5	111	2.929	0.7072	12.5
JCPDS 98-009-1204	30.4	111	2.934	—	

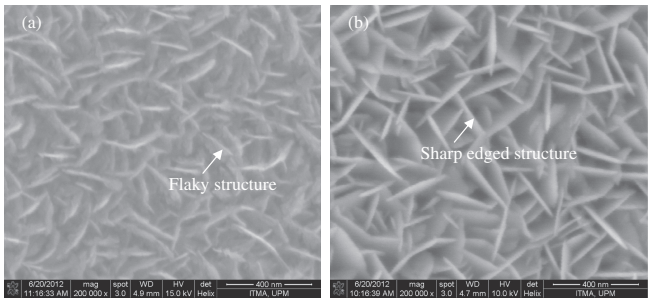

Figure 3. SEM images for surface morphology of (a) Without-AGC and (b) With-AGC of SnSe thin films.

3.2 Surface morphology

Based on profilometric measurements, thickness values for SnSe thin films measured from 2 pieces each, prepared With- and Without-AGC, were 415, 442 nm and 521, 548 nm, respectively. The With-AGC films are less thick than the With-AGC films. The collisions between Sn and Se atoms/ions with argon gas during deposition lower the deposition rate. Since starting amount (0.1 g) of SnSe powder was same, smaller thickness for With-AGC is expected in same deposition time.

The surface morphology of the SnSe thin films was studied using FESEM. Figure 3 shows the micrographs of With- and Without-AGC SnSe thin films. The Without-AGC film shows a dull and flaky

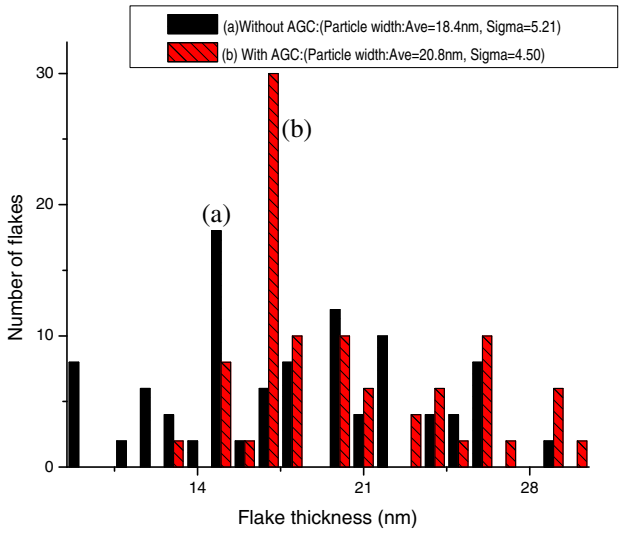

Figure 4. (Color online) Flake thickness distribution for (a) Without-AGC and (b) With-AGC SnSe thin films.

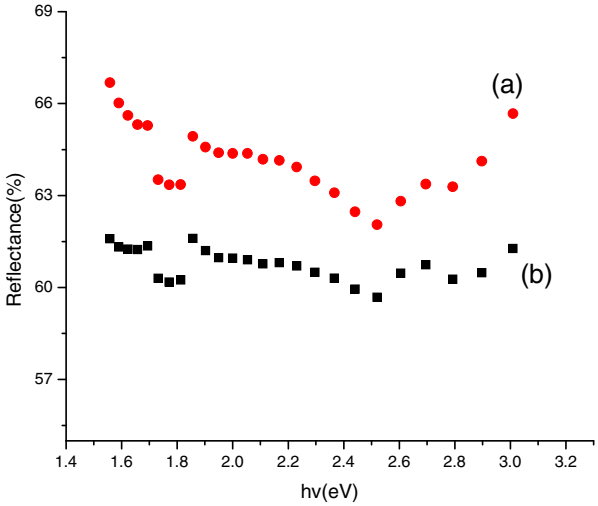

Figure 5. (Color online) Plots of reflectance vs. photon energy for (a) Without-AGC and (b) With-AGC SnSe thin films.

structure. The With-AGC film showed a similar flake structure but having sharper edges. The SEM images indicate that the With-AGC film has higher uniformity than that of the Without-AGC film. Figure 4 shows distributions of the flake thickness values in both films. The histogram data were obtained from direct measurement of each thickness with representative group of 50 flakes on FESEM photograph. On the average, the With-AGC flakes were thicker (20.8 nm, $\sigma = 4.50$) with narrower distribution compared to Without-AGC counterpart (18.4 nm, $\sigma = 5.21$).

The results show significant morphological differences between the With-AGC and the Without-AGC systems. Nucleation and growth condensation taking place under argon gas atmosphere are responsible for the differences not only in crystallinity but in surface morphology as well. To further confirm if the significant morphological differences between the With-AGC and Without-AGC affected the electrical conductivity, the PEC study and stability tests were conducted as described below.

3.3 Optical properties

Optical properties of both SnSe thin films were studied, by measuring their reflectance and absorbance spectra. Figure 5 shows reflectance spectra measured for both films. The reflectance of the

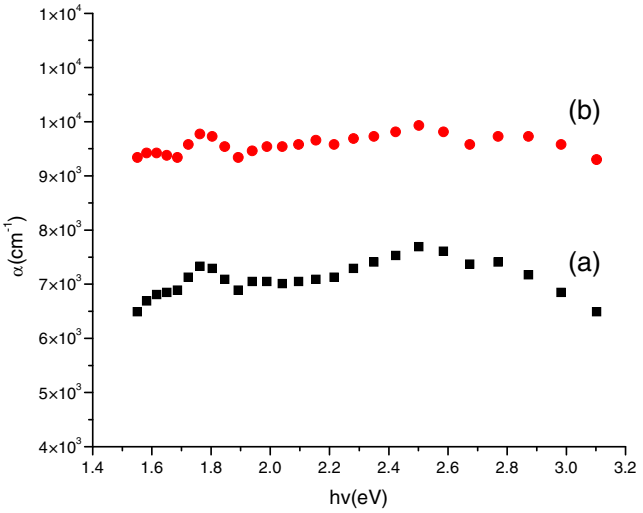

Figure 6. (Color online) Plots of absorption coefficient value vs. photon energy for (a) Without-AGC and (b) With-AGC SnSe thin films.

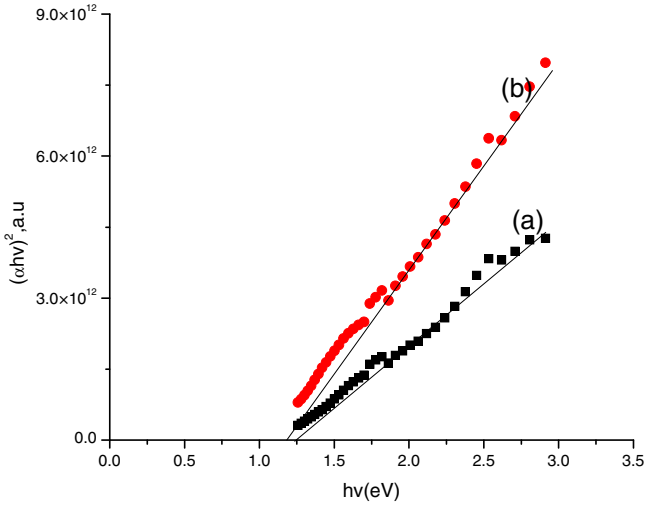

Figure 7. (Color online) Optical absorption spectra as, $(\alpha h\nu)^2$ versus photon energy plots, for (a) Without-AGC and (b) With-AGC SnSe thin films.

With-AGC film was lower than the Without-AGC. The sharp edged surface structure of the With-AGC film probably suppressed the reflectance. Decreasing the reflectance is one preferable feature of opto-electric devices.

The absorption coefficient, α (cm^{-1}), was calculated from the measured value of absorbance, A, using the formula, $\alpha = 2.303\,A/t$, where t was film thickness (cm). Figure 6 shows the absorption coefficient spectra for the Without- and With-AGC films. The values for the Without- and With-AGC films were 7×10^3 and 1×10^4 cm^{-1}, respectively. The With-AGC film exhibited higher absorptivity than the Without-AGC film due to its higher crystallinity and uniformity. As a result, the higher absorption coefficients of the With-AGC film promote more photon absorption, which excites more electrons into conduction band and generates more holes in valence band. This increases photoactivity of the electrode.

The optical energy band gap of the SnSe thin film was determined using the relation $\alpha h\nu = B(h\nu - E_g)^n$, where B is a constant, hν is the incident photon energy (eV), and E_g is the optical energy band gap (eV). The exponent n depends on the type of optical transition in a material. Since the majority transition of SnSe is a direct allowed transition, n equals 1/2. Thus the optical energy band gap values for With- and Without-AGC films were determined by plotting $(\alpha h\nu)^2$ versus (hν) and extrapolation to $\alpha h\nu = 0$ as shown in Fig. 7. The measured direct optical band gap decreases from 1.26 eV (Without-AGC) to 1.19 eV (With-AGC). The band gap values decreased with decreasing FWHM as the crystallite sizes of the film increased. The band gap of the With-AGC film is consistent with literature value ($E_g = 1.21$ eV) for systems prepared by a reactive evaporation,[18] whose film exhibited soundly good crystallinity.

3.4 Photoelectrochemical performance

A PEC cell configuration SnSe|$[Fe(CN)_6]^{3-}$, $[Fe(CN)_6]^{4-}$|Pt was constructed to study the PEC characteristics, with special attention paid to electrode photoresponse and stability. Dark current density vs. potential (J_D-V) plots and overall illumination current density vs. potential (J_I-V) plots (using 0.1 W/cm^2), are shown in Fig. 8. At potentials more positive than +0.25 V (vs. Ag/AgCl), positive dark current flows for both film electrodes (With- and Without-AGC), and the current increased as potential goes more positive. On the other hand, under the potential region less positive than +0.25 V (vs. Ag/AgCl) negative leakage current continued to flow in cases of both electrodes. The J_D-V behavior indicates that the electrodes

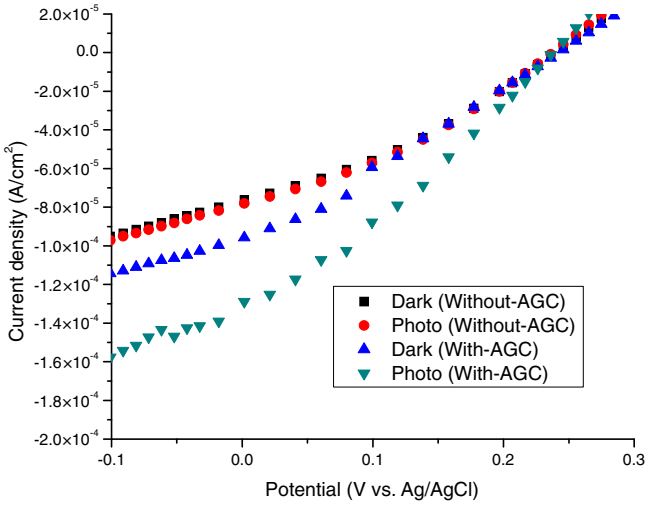

Figure 8. (Color online) Effect of argon gas on J-V characteristics for SnSe thin film electrodes.

are p-type semiconductors.[25] Under illumination, the negative photocurrent flows at potentials more negative than the open circuit potential ($V_{OC} = +0.25$ V) in both electrodes. This behavior is also typical for p-type semiconductor working electrodes[26] and is consistent with earlier reports for SnSe electrodes.[5,9,27,28] However, both electrodes showed negative leakage currents in the dark at potentials more negative than the onset potential (Vonset), which is normally encountered in thin film electrodes.

Figure 9 shows net photo current density vs. potential (J_p-V) plots, calculated by subtracting the J_D-V plots from the J_I-V plots for both With- and Without-AGC film electrodes. The absolute photo current density $|J_p|$ of the With-AGC electrode was more than ten times higher than that for the Without-AGC electrode. This enhancement cannot be justified based on higher absorption efficiency of the With-AGC film only, since the With-AGC film absorption coefficient is only twice that for the Without-AGC film. Higher current density values and photorespone indicate lower resistance, better charge separation and higher charge transfer across the solid/redox couple interface, in case of the With-AGC system. All such characteristics are due to enhanced crystallinity (including larger crystallite size) and surface morphology exhibited by the With-AGC film electrodes, as discussed above.

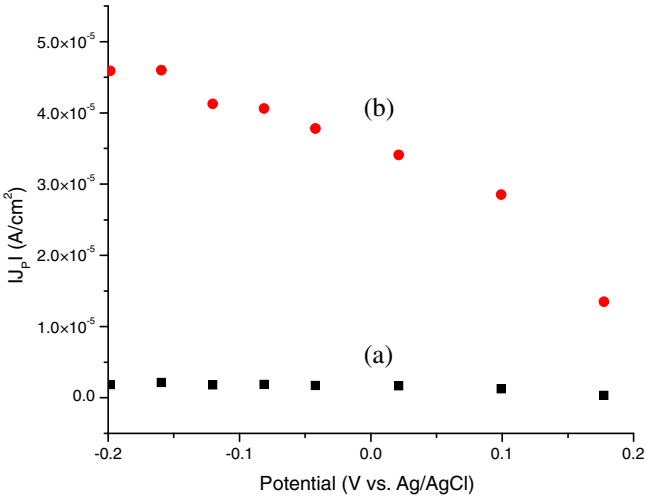

Figure 9. (Color online) Absolute photo current density $|J_P|$; difference between the illumination current density (J_I) and dark current density (J_D) for (a) Without-AGC and (b) With-AGC SnSe thin film electrodes.

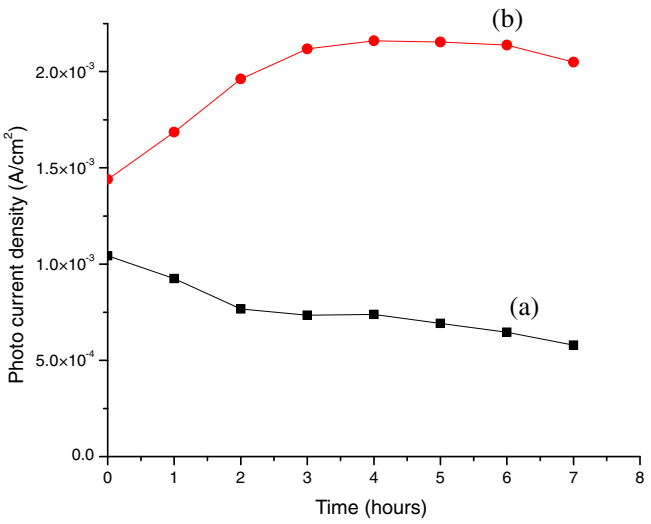

Figure 10. (Color online) Plots of absolute short-circuit current density vs. time measured for (a) Without-AGC and (b) With-AGC SnSe thin film electrodes.

Stabilities of both electrode systems were studied by monitoring the value of short circuit current density under steady illumination intensity over a period of 7 hours, with zero applied potential, Fig. 10. The absolute current density value measured for the With-AGC film increased at the beginning, and then reached a steady value with time, while in the Without-AGC system, the value continued to decrease with time. The With-AGC film electrode exhibited relatively small initial value of current density, which is due to presence of foreign matters (impurities) at the electrode surface. Such matters degrade away with time, leaving clean surfaces with higher charge transfer across the solid/liquid interface and higher current density. The electrode then exhibited steady value for current density showing sound stability with time. Similar behaviors have been reported for different systems.[29] The Without-AGC film, with lower crystallinity and surface uniformity, continued to degrade, without showing enough stability with time. The higher stability of the With-AGC electrode is attributed to its higher crystallinity and surface uniformity compared to the Without-AGC counterpart, as discussed above.

Inclusion of argon gas thus enhanced crystallite sizes, crystallinity and surface morphology of the SnSe electrodes, which in turn enhanced its PEC characteristics. The argon gas effect resembles that of annealing thin film electrodes of different materials, commonly reported in literature.[30,31] Metal chalcogenide-based photoelectrodes are no exception, and their PEC characteristics can be enhanced by annealing and modifying their crystallinity and surface morphology/texture.[1,26,31] This lowers recombination by removing trap sites inside the grains and at the grain boundaries. Moreover, charge transfer at the solid/liquid interface would be enhanced yielding higher short circuit current density. In this work, the photoactivity (value of photocurrent at 0 potential) was increased to about 20 fold when using the AGC method compared to the Without-AGC as a reference, Fig. 9.

The introduction of argon gas inside the evaporation chamber during thermal vacuum evaporation process is responsible for the enhancement of the PEC system. It is therefore recommended to use such technique for thin film electrode preparations, as only one step preparation is needed to enhance the electrode crystallinity. Research is underway here to investigate the combined effects of argon gas inclusion during film preparation, followed by annealing the resulting film.

4. Conclusion

Inclusion of argon gas enhanced crystallinity and morphology of SnSe thin films, deposited onto ITO/glass by vacuum thermal evaporation, as observed from XRD and FESEM. SnSe thin film electrodes prepared using argon gas exhibited higher photocurrent density, photosensitivity and stability in ferricyanide/ferrocyanide redox couple systems. The enhancement in thin film electrode crystallinity, morphology and PEC characteristics is due to slower film growth rate when using argon gas. The results show the added value of using argon gas in future thin film electrode preparations even without annealing. The combined effects of using argon gas during film preparation, followed by annealing, on PEC characteristics, are worth to study.

Acknowledgment

Support donated by the Ministry of Higher Education of Exploratory Research Grant Scheme Grant No. 5527051 and UPM Research Grant Scheme is acknowledged.

References

1. P. P. Hankare, P. A. Chate, D. J. Sathe, M. R. Asabe, and B. V. Jadhav, *Solid State Sci.*, **10**, 1970 (2008).
2. O. Savadogo and K. C. Mandal, *Mater. Chem. Phys.*, **31**, 301 (1992).
3. P. P. Hankare, P. A. Chate, P. A. Chavan, and D. J. Sathe, *J. Alloys Compd.*, **461**, 623 (2008).
4. M. Fujii, T. Kawai, and S. Kawai, *Sol. Energy Mater.*, **18**, 23 (1988).
5. Z. Zainal, N. Saravanan, K. Anuar, M. Z. Hussein, and W. M. M. Yunus, *Mater. Sci. Eng., B*, **107**, 181 (2004).
6. A. C. B. Silva, A. F. Mesquita, E. M. Neto, and A. O. Porto, *Solid State Commun.*, **135**, 677 (2005).
7. R. Indirajith, T. P. Srinivasan, K. Ramamurthi, and R. Gopalakrishnan, *Curr. Appl. Phys.*, **10**, 1402 (2010).
8. N. D. Boscher, C. J. Carmalt, R. G. Palgrave, and I. P. Parkin, *Thin Solid Films*, **516**, 4750 (2008).
9. N. R. Mathews, *Sol. Energy*, **86**, 1010 (2012).
10. C. B. Roy, D. K. Nandi, and P. K. Mahapatra, *Electrochim. Acta*, **31**, 1227 (1986).
11. M. Z. Xue and Z. W. Fu, *Electrochim. Acta*, **52**, 988 (2006).
12. H. Benelmadjat, B. Boudine, O. Halimi, and M. Sebais, *Opt. Laser Technol.*, **41**, 630 (2009).
13. C. C. Koch, *Nanostructured Materials: Processing, Properties, and Applications*, 2nd Ed., William Andrew, Inc., p. 47 (2007).
14. N. Sabli, Z. A. Talib, W. M. M. Yunus, Z. Zainal, H. S. Hilal, and M. Fujii, UKM, Kuala Lumpur, Malaysia, December 5–7, 2012, The 3rd ISESCO International Workshop and Conference on Nanotechnology, p. 105 (2012).

15. B. Subramanian, T. Mahalingam, C. Sanjeeviraja, M. Jayachandran, and M. J. Chockalingam, *Thin Solid Films*, **357**, 119 (1999).
16. Y. Z. Li, X. D. Gao, C. Yang, and F. Q. Huang, *J. Alloys Compd.*, **505**, 623 (2010).
17. R. Mariappan, M. Ragavendar, and G. Gowrisankar, *Chalgogenide Lett*, **7(3)**, 211 (2010).
18. K. J. John, B. Pradeep, and E. Mathai, *J. Mater. Sci.*, **29**, 1581 (1994).
19. R. C. Sharma and Y. A. Chang, *J. Phase Equilib.*, **7**, 68 (1986).
20. N. Kumar, V. Sharma, N. Padha, N. M. Shah, M. S. Desai, C. J. Panchal, and I. Y. Protsenko, *Cryst. Res. Technol.*, **45**, 53 (2010).
21. Z. Zainal, S. Nagalingam, A. Kassim, M. Z. Hussein, and W. M. M. Yunus, *Mater. Sci.*, **21**, 225 (2003).
22. V. Hass, H. Gleiter, and R. Birringer, *Scr. Metall. Mater.*, **28**, 721 (1993).
23. A. C. B. Silva, A. F. Mesquita, E. M. Neto, A. O. Porto, G. M. Lima, J. D. Ardisson, and F. S. Lameiras, *Solid State Commun.*, **135**, 677 (2005).
24. S. Gayathri, S. Muthumari, S. Arockia, G. Devi, R. Vijayalakshmi, and C. Sanjeeviraja, *J. Appl. Sci.*, **12**, 1706 (2012).
25. H. Gerischer, *Physical Chemistry: An Advanced Treatise* (Ed. H. Eyring), Academic Press, New York, NY, Vol. IXA, p. 463 (1970).
26. Z. Zainal, S. Nagalingam, A. Kassim, M. Z. Hussein, and W. M. M. Yunus, *Sol. Energy Mater. Sol. Cells*, **81**, 261 (2004).
27. M. Sharon and K. Basavaswaran, *Sol. Cells*, **20**, 323 (1987).
28. G. H. Chandra, J. N. Kumar, N. M. Rao, and S. Uthanna, *J. Cryst. Growth*, **306**, 68 (2007).
29. H. S. Hilal, W. Ateereh, T. Al-Tel, R. Shubaitah, I. Sadeddin, and G. Campet, *Solid State Sci.*, **6**, 139 (2004).
30. R. K. Pandey, S. Mishra, S. Tiwari, P. Sahu, and B. P. Chandra, *Sol. Energy Mater. Sol. Cells*, **60**, 59 (2000).
31. H. S. Hilal, R. M. A. Ismail, A. El-Hamouz, A. Zyoud, and I. Saadeddin, *Electrochim. Acta*, **54**, 3433 (2009).